Simulations of Snow Physicochemical Properties in Northern China using WRF-Chem

Xia Wang[1], Tao Che[2,3], Xueyin Ruan[1], Shanna Yue[2,3], Jing Wang[2,3], Chun Zhao[1,4,5*], Lei Geng[1,4,5*]

5

[1]School of Earth and Space Sciences, University of Science and Technology of China, Hefei 230026, Anhui, China

[2]Key Laboratory of Remote Sensing of Gansu Province, Heihe Remote Sensing Experimental Research Station, Northwest Institute of Eco-Environment and Resources, Chinese Academy of Sciences,

10 Lanzhou 730000, China

[3]College of Resources and Environment, University of Chinese Academy of Sciences, Beijing 100049, China

[4]Deep Space Exploration Laboratory, Hefei 230088, Anhui, China.

15 [5]CAS Center for Excellence in Comparative Planetology, University of Science and Technology of China, Hefei 230026, Anhui, China

Correspondence to: Lei Geng (genglei@ustc.edu.cn) and/or Chun Zhao (chunzhao@ustc.edu.cn)

Abstract. Snow is a key component of the cryosphere and has significant impacts on surface energy balance, hydrology, atmospheric circulation, and etc. In addition, numerous studies have indicated that

20 snow impurities, especially nitrate, are sensitive to sunlight and can be photolyzed to emit reactive species including NO_2 and HONO, which serve as precursors of O_3 and radicals and disturb the overlying atmospheric chemistry. This makes snow a reservoir of reactive species, and this reservoir is particularly important in remote and pristine regions with limited anthropogenic emissions. The magnitude of snow chemical emissions is also influenced by snow physical properties, including snow

25 depth, density and concentrations of light-absorbing impurities (e.g., BC and dust). Exploring and elucidating the emissions and atmospheric consequences of the snow-sourced reactive species require a global or regional model with a snow module. Here, we parameterized atmospheric nitrate deposition and its distributions in snow using a regional chemical transport model, i.e., the WRF-Chem (Weather Research and Forecasting Model coupled with Chemistry) model, and evaluated the performance of the

30 WRF-Chem model in simulating snow cover, snow depth, and BC, dust and nitrate concentrations with field observations in northern China which is one of the regions with dense and prolong snow cover. The model reasonably reproduces the observed snow cover and depth in northeastern and northwestern

China, and the observed snow dust and nitrate concentrations are also reasonably reproduced. These

results illustrate the ability of WRF-Chem in simulating snow properties including concentrations of

35　reservoir species in northern China, and in the future, we will incorporate snow nitrate photolysis in the

model, exploring the emissions of snow NO_x from nitrate photolysis and the impacts on local to

regional atmospheric chemistry and air pollutant transformations.

1 Introduction

40　　　Through the effects on surface albedo and energy balance, snow cover has important impact on

Earth's climate system (Flanner et al., 2011). In particular, the snow's depth, grain size, and impurities

can affect its albedo, which in turn significantly influences surface warming as a result of the swift

feedback on snow structure, snow sublimation rates, and snow melt rates (He et al., 2018; Picard et al.,

2012). What is more, snow is also significant in atmospheric chemistry. Under appropriate conditions

45　(e.g., illuminated by sunlight), photolysis of snow impurities can lead to the release of reactive species,

including nitrogen oxides ($NO + NO_2 = NO_x$) and reactive halogens, to the overlying atmosphere,

disturbing atmospheric chemistry (Dominé and Shepson, 2002; Grannas et al., 2007; Zatko et al.,

2016a). Improving the understanding of the spatiotemporal variations in snow physical and chemical

properties is thus important for assessing the effects of snow cover on climate and atmosphere

50　environment.

　　　As one of the major chemicals in snow, nitrate is perhaps one of the most important reactive

species. In particular, snow nitrate is active under sunlight, and its photolysis results in emissions of

NO_x and also HONO into the boundary atmosphere (Chu and Anastasio, 2003; Zatko et al., 2013; Chen

et al., 2019; Barbero et al., 2021). In pristine regions with snow cover, long-range transported

55　atmospheric nitrate deposited and preserved in snow could serve as a potentially important secondary

source of NO_x, which is important for local production of O_3 and OH radicals (Bouwman, 1998; Hall

and Matson, 1999; Li et al., 2015; Logan, 1983; Nelson et al., 2023). The latter are important for

atmospheric reactivity, or more specifically, the so-called atmospheric oxidation capacity. Previous

studies have investigated the photolysis of snow nitrate in polar regions. For example, when

60　considering the emissions of NO_x from snow nitrate photolysis, there is a potential doubling of O_3

levels and significant increases of 5 to 6 times in the level of OH in the overlying atmosphere in

Greenland and Antarctica (Zatko et al., 2016a). In addition to polar regions, Zatko et al. (2016b)

investigated the effects of snowpack emissions on local atmospheric chemistry in a north American site located at midlatitudes but with extensive snowfall in winter. They also found significant emissions of NO$_x$ from snow, although the contribution to the local NO$_x$ budget was relatively small given that extensive anthropogenic emissions persist at the studied site, originating from traffic related to oil and natural gas extraction activities. At another mid-latitude site, Kalamazoo, Michigan, Chen et al. (2019), observed up to 44% higher HONO levels in a snowy urban environment than in other regions without snow. The high HONO concentration is in part due to snow nitrate photolysis, and the subsequent photolysis of HONO produces OH, which serves as another important OH source in addition to the common O$_3$ photolysis channel.

Northern China is renowned as one of the regions with the densest winter snow cover, boasting a broad extent of snow coverage that can reach 85% (Zou et al., 2022). Moreover, the duration of snow cover is notably extensive, with certain frigid areas experiencing snow coverage for as long as 120-140 days per year (Wang and Chen, 2022). Compared to those in polar regions, the snow in this region has higher nitrate concentrations (i.e., 0.1 - 30 µg g^{-1}, ~ three orders of magnitude higher than those in polar regions (0.1 - 200 ng g^{-1}) (An et al., 2022; Legrand and Mayewski, 1997; Wendl et al., 2015; Zhang et al., 2013; Jiang et al., 2021)) and can receive more actinic fluxes. These conditions may facilitate snow nitrate photolysis, making it a potentially important source of NO$_x$ and HONO, which are limited from other sources in winter due to low human and bacterial activities in snow-covered regions. In addition, the prevailing northern wind in winter would transport snow-sourced NO$_x$ and/or the subsequent enhanced atmospheric O$_3$ and other species to downwind regions, including the northern China Plain (NCP), where severe haze and O$_3$ pollution occur frequently in winter. However, whether snow emission can influence atmospheric chemistry and air quality in downwind regions remains to be further investigated.

Moreover, quantifying the snow emissions of reactive species and the impacts on the overlying atmosphere as well as downwind regions requires an atmospheric chemical transport model with snow modules that can simulate snow physical and chemical properties, including snow cover, snow depth and snow impurities (e.g., BC, dust, and nitrate concentrations), and also be able to calculate the radiative transfer of actinic flux in snow, the associated snow photochemistry and the emissions of reactive species into the overlying atmosphere. Zatko et al. (2016a) have added a NO$_3^-$ photolysis parameterization to a global chemical transport model, that is the Goddard Earth Observing System

(GEOS) Chemistry model (GEOS-Chem). However, as an offline model, GEOS-Chem uses archived meteorological fields, which generally have coarse resolutions, and errors can be caused by regional or smaller-scale simulations (Yu et al., 2018); moreover, GEOS-Chem cannot simulate meteorological-chemical interactions, which may be important for modeling or forecasting snow cover changes and their impacts on local to regional climate and atmospheric chemistry. Therefore, we plan to utilize the WRF-Chem model, which is an advanced, on-line regional chemistry model with a relatively well-developed snow module. However, before doing that, we have to first incorporate snow nitrate simulations into the model, which is currently not included in the snow module, and evaluate the ability of WRF-Chem in simulations of snow physicochemical properties in northern China. Therefore, this study serves as an evaluation on the performance of WRF-Chem simulations of snow coverage and snow physicochemical properties in northern China, with a development on the modeling of snow nitrate concentrations. This is the first step to use the model to investigate the effects of snow cover on local to regional atmospheric chemistry.

2 Model description and parameterizations

2.1 WRF-Chem

We use the version (v3.5.1) of WRF-Chem updated by the University of Science and Technology of China in this study. Distinguished from the version that is available to the public, the USTC iteration boasts supplementary functionalities, including the online diagnosis of aerosol-specific radiative forcing and the aerosol-snow albedo effect (Zhao et al., 2014; Zhao et al., 2013a; Du et al., 2020). The aerosol scheme employed is the Model for Simulating Aerosol Interactions and Chemistry (MOSAIC – 8 bins) (Zaveri et al., 2008), and the gas-phase chemistry mechanism is the Carbon Bond Mechanism Z (CBM-Z) (Zaveri and Peters, 1999), both of which are used in this iteration of WRF-Chem. The model considers main aerosol components including nitrate (NO_3^-), sulfate (SO_4^{2-}), chloride (Cl^-) ammonium (NH_4^+), black carbon (BC), dust, and sea salt, and mineral dust. When simulate the generation and growth of aerosols, the MOSAIC mechanism takes into account a variety of chemical and physical processes, including but not limited to gas-to-particle conversion, particle nucleation, coagulation, condensation, and evaporation. Additionally, the model considers important processes of aerosol deposition, including both dry and wet deposition. These processes are critical for comprehending the behavior and fate of aerosols, including their incorporation in snow. In the model, particle diffusion and

gravitational effects are considered to simulate dry deposition of aerosol (Binkowski and Shankar, 1995). Wet deposition, including rainout, washout and scavenging processes, is also simulated in the

125 model to accurately represent the removal of aerosols through precipitation following the methodologies outlined by Easter et al. (2004) and Chapman et al. (2008). This research does not explicitly model cloud-ice-borne aerosols. However, it does consider the elimination of aerosols as they undergo freezing within droplets. The removal of aerosols by convection and their wet deposition via cumulus clouds are modeled according to the methods described by Zhao et al. (2013b). This study

130 utilizes the Community Land Model (CLM) v4.0 (Lawrence et al., 2011) coupled with the Snow, Ice, and Aerosol Radiative Model (SNICAR) (Flanner and Zender, 2005) as an option for the land surface model (Jin and Wen, 2012).

Table 1. An overview of the model configurations utilized.

Option	Parameterization schemes
Simulation periods	October 2017 to March 2018
Horizontal resolution	36 km
Model spin-up time	2 months
Vertical levels	41 (About 8 layers beneath the surface of 1 km)
Domain sizes	149 × 189
Photolysis scheme	Fast - J
Aerosol chemistry	MOSAIC 8 bin
Gas-phase chemistry	CBM-Z
Land surface scheme	CLM land surface scheme
Microphysics	Morrison 2-moment
Longwave Radiation	RRTMG
Shortwave Radiation	RRTMG
Planetary boundary layer	YSU
Cumulus Cloud	Kain–Fritsch

135

2.2 Snow simulations in WRF-Chem

Snow accumulations on land surface as well as the physicochemical properties are calculated using SNICAR model in WRF-Chem. This mode incorporates a layered structure, considering the vertical variability of snow properties and accounting for the heating effects of the underlying ground

140 and its influence on snow characteristics (Flanner et al., 2012; Flanner and Zender, 2005; Flanner et al., 2009; Flanner et al., 2007). The theoretical framework of Wiscombe and Warren (1980) and the two-stream, multi-layer radiative scheme proposed by Toon et al. (1989) are employed within SNICAR. It has excellent performance in simulating snow surface albedo, radiative absorption within snow layers, snow impurities, and radiative effects within snow. It was initially utilized by Flanner et al. (2007) to

145 investigate snow aging and aerosol heating in a global climate model. The simulated changes in snow albedo based on specific black carbon (BC) concentrations have been validated through field measurements and laboratory experiments (Brandt et al., 2011; Hadley and Kirchstetter, 2012). In CLM, there are five thermal layers that correspond to the radiative layers defined by SNICAR, enabling the vertical resolution of densification, snow meltwater transport, and thermal processes

150 (Oleson et al., 2010a). For a more comprehensive understanding of the SNICAR model, refer to Flanner and Zender (2005) and Flanner et al. (2012); (Flanner et al., 2007).

To simulate snow nitrate photolysis and its impacts on overlying atmospheric chemistry, one needs to obtain snow cover, snow depth, and snow physical and chemical properties, including snow density; impurities, including BC, dust; and nitrate. Physical properties are used to simulate radiative transfer in

155 snow, and the nitrate concentration determines the photolysis rate of nitrate and thus the release of snow-sourced NOx. All others are already included in SNICAR; for instance, BC and dust have been parameterized by Zhao et al. (2014). However, this approach does not involve the calculation of nitrate in snow. In this study, we parameterized the snow nitrate concentrations.

160 **2.2.1 Parameterization of nitrate concentrations in snow**

Currently, SNICAR does not include calculations of nitrate concentrations embedded in snow. In principle, concentrations of nitrate within each snow layer can be influenced by atmospheric deposition flux, new snowfall, layer combinations and divisions, and, in a rare case, meltwater flushing. The processes of atmospheric nitrate incorporation in snow in the atmosphere include in-cloud and below-

165 cloud scavenging of particulate and gaseous nitrate. In-cloud scavenging (rainout) refers to the incorporation of aerosols and gases into snow during its formation in the atmosphere. Below-cloud scavenging (washout), on the other hand, occurs when snow falls to the surface, and particulate and gaseous nitrates are scavenged by snow. In addition, dry depositions of particulate and gaseous nitrate can directly lead to accumulations of nitrate in surface snow. These processes together result in the

170 accumulation of nitrate in snow. In this study, wet deposition of atmospheric nitrate was estimated

using the predictive precipitation method, which helps prevent any discrepancies from predetermined

nitrate deposition and meteorological conditions (Zhao et al., 2014). The SNICAR model considers the

transport, settling, and deposition processes of particulate nitrates of different types and sizes in the

atmosphere.

175 The dry deposition fluxes of atmospheric nitrate on the snow surface (kg m^{-2} s^{-1}) are calculated as

follows:

$$F_{dry} = V_{no3} \times C_{no3} \times D_{air} \tag{1}$$

where V_{no3} is the dry deposition velocity of particulate or gaseous nitrate (m s^{-1}), C_{no3} is the

atmospheric concentration of particulate or gaseous nitrate (particulate: μg kg-dryair^{-1}; gaseous: ppmv),

and D_{air} is the air density (kg m^{-3}). The wet deposition fluxes of atmospheric nitrate (kg m^{-2} s^{-1}) were

180 calculated using the following equations:

$$F = \frac{(C_{no3} \times D_{air} \times H_{air})}{dt} \tag{2}$$

$$F_{wet} = F_{before} - F_{after} \tag{3}$$

where H_{air} is the thickness of the atmospheric layers (m), dt is the time step in model (s), and C_{no3} and

D_{air} are the same as mentioned above. F represents the instantaneous mass concentration at each time

step in the atmosphere. The wet deposition fluxes of atmospheric nitrate were calculated by subtracting

F recorded before and after the large-scale wet removal process in the atmosphere.

185 After deposition, nitrate is assumed to quickly mix well within the top 2cm layer. The nitrate mass

concentration in surface snow (M_{NITS}: kg kg^{-1}) was calculated by deposition fluxes of atmospheric

nitrate as follows:

$$M_{NITS} = \frac{\left((F_{dry} + F_{wet}) \times dtime \right)}{W_{sno}} \tag{4}$$

where $dtime$ is the land model time step used in SNICAR(s), as distinct from the dt mentioned above

used in atmospheric processes, and W_{sno} is the snow mass in the surface layer (kg m^{-2}). Furthermore,

190 the CLM continuously builds a new surface snow layer when a fresh snowfall event occurs, and nitrate

mass concentrations in surface snow are updated as follows:

$$M_{NITS}^{new} = M_{NITS} + \frac{\Delta F \times dtime}{\Delta W_{sno}} \Delta t \tag{5}$$

where ΔF is the cumulative wet and dry deposition of atmospheric nitrate during the entire period

between the newly fallen snow and the previous time step, $\Delta Wsno$ is the newly gained snow mass

during the entire period between the newly fallen snow and the previous time step, and Δt is the period
spanning from the newly fallen snow to the previous time step.

By repeating the above motioned processes, a snowpack with initial nitrate concentrations in each
layer of the snowpack was simulated.

2.2.2 Potential modification by melting processing after deposition

Previous studies have shown that at midlatitudes, snow melt occurs occasionally, which will
modify the concentrations of impurities (Zhao et al., 2014; Flanner et al., 2007; Eichler et al., 2001).
Following similar processes, we considered the potential effects of these processes on snow nitrate
concentrations. In particular, the melting of snow can redistribute nitrate (and other species) through the
introduction of excess water into the layer beneath when the meltwater surpasses the layer's retention
capacity, which is determined by irreducible water saturation and snow porosity. The rate of change in
nitrate mass for each layer i, due to its incorporation into meltwater, is directly proportional to the mass
mixing ratio and with the adjustment of a scavenging factor, which can be described as follows:

$$\frac{dm_i}{dt} = k(q_{i+1}c_{i+1} - q_i c_i) + D \tag{6}$$

where m_i represents the total mass of nitrate within layer i, which is affected by the removal efficiency
(k) and the water flux leaving the layer (q_i). The concentration of nitrate in layer i, denoted as c_i, is the
proportion of the nitrate mass to the total mass of water in both liquid and solid forms within that layer.
D represents the combined effect of total atmospheric particulate and gaseous nitrate deposition, which
is specifically added to the surface layer of the snowpack. This study assigned a scavenging ratio for
nitrate of 0.20. However, the scavenging ratios of aerosol species in snow remain highly uncertain and
require further refinement through supplementary observations. (Flanner et al., 2012; Qian et al., 2014;
Zhao et al., 2014); Nonetheless, compared to the values used in observations reported elsewhere
previously, the value we used is rational (Doherty et al., 2013; Moore et al., 2005). It is worth noting
that the portion of nitrate mass lost through meltwater from the bottom layer of snow is considered to
be removed from the snowpack and is not accounted for within the model.

In summary, the nitrate concentrations in each snow layer are determined by factors such as
atmospheric deposition rates, the amount of new snowfall, layer combinations and divisions, and
meltwater flushing (Oleson et al., 2010b; Flanner et al., 2012; Flanner et al., 2007). When snow layers

are combined or divided, nitrate masses are redistributed proportionately with snow masses conserving nitrate masses within the snow column.

225 **2.3 Numerical experiments**

The study employed simulations covering the entire area of China, utilizing a spatial resolution of 36×36 km with a grid composed of 149×189 cells, as depicted in Fig. S1. The simulations run from December 2017 to March 2018 covering the field campaign period, with an additional two months modeled before December 2017 as the model spin-up. The starting and side boundary conditions for

230 meteorology are drawn from the NCEP Final reanalysis dataset, which provides data at a resolution of $1°$ horizontally and at 6-hour intervals. The specific model setup employed in this research is outlined in Table 1, including the Yonsei University (YSU) planetary boundary layer scheme, the Kain-Fritsch cumulus parameterization scheme, the Morrison two-moment microphysics scheme, the Rapid Radiative Transfer Model (RRTMG) for both longwave and shortwave radiation, and the Community

235 Land Model (CLM) for land surface processes. The YSU scheme was chosen to parameterize the planetary boundary layer processes, while the Kain-Fritsch scheme addresses the representation of convective clouds. The Morrison scheme handles microphysical processes, capturing the characteristics of cloud and precipitation formation. The RRTMG schemes accurately modeled longwave and shortwave radiation interactions. Finally, the CLM scheme accounted for land surface interactions. By

240 integrating these schemes, this study aimed to provide comprehensive simulations and insights into the atmospheric and snow processes and interactions involved during the selected period.

For the purpose of modeling anthropogenic emissions, we utilize the 2015 version of the Multi-resolution Emission Inventory for China (MEIC), which offers a fine resolution of $0.1° \times 0.1°$ (Li et al., 2017a; Li et al., 2017b). To determine the vertical distribution of dust, we apply the GOCART dust

245 emission scheme developed by Ginoux et al. (2001). Subsequently, the generated dust particles are assigned to numerous size categories within the MOSAIC aerosol scheme, adhering to the scale-invariant fragmentation mechanics for brittle materials as described by Kok (2011). Additional information regarding the integration of the dust emission scheme with the MOSAIC aerosol scheme in WRF-Chem is available in Zhao et al. (2010). Hourly resolved biomass burning emissions, with a 1 km

250 horizontal resolution, are obtained from the Fire Inventory from NCAR (FINN) (Wiedinmyer et al., 2011). Biogenic emissions were calculated using the MEGAN v2.0 model.
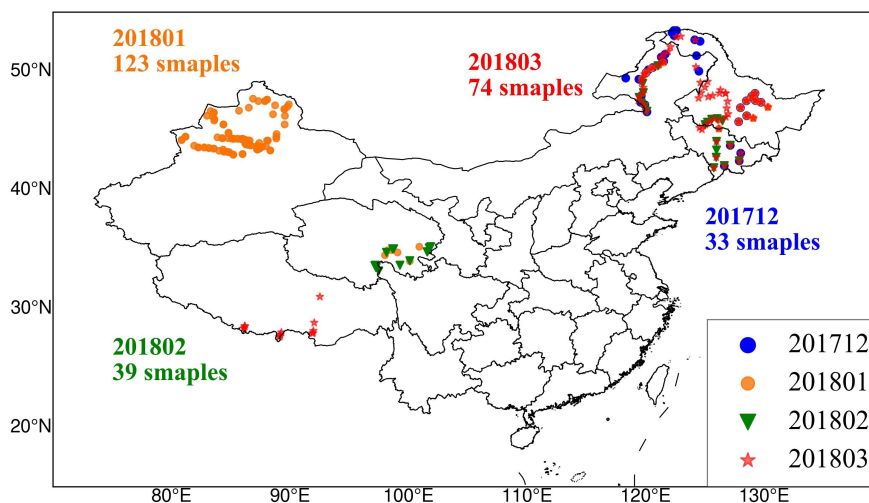
2.4 Observations

2.4.1 Snow and its physicochemical properties datasets

255   The main dataset for observing and assessing the simulations of snow and its physicochemical properties was obtained from the field study conducted by Che et al. (2022) from December 2017 to March 2018, when snow was collected from more than 200 road trips in both the Northeast and Northwest regions of China. The observational route in Fig. 1 covers three distinct regions with different climatic zones, underlying surfaces, and elevations. Extensive field observations were

260   conducted to study snow cover characteristics along this route. The sampling points are labeled in Fig. 1 and categorized by region and month. At each site, snow samples were collected. A total of 269 snow samples were collected, and the concentrations of nitrate and calcium and the snow depth were measured.

For further information regarding the measurements conducted during the Northern China

265   campaign, additional details are available in Che (2020). During the campaign, snow samples were collected at various depths, yet the concentration of ions was chiefly calculated for the top layer of the snow. Hence, we compare the simulated ion mass content within the uppermost 2 cm of the surface snow layer against the average observational data derived from snow samples collected at depths ranging from 2 to 5 cm.

observation station sites

270

Figure 1. Sampling points along the road trip from December 2017 to March 2018 are marked with different colors to represent different months. Color indicates different months of the observations.

2.4.2 MODIS-based snow area product dataset

275   In addition to field observations of snow impurities and depth, we also collected snow cover data for comparison with the model simulations. For this study, we utilized the daily cloud-free 500 m snow cover dataset over China, compiled by Hao et al. (2022). This dataset is provided as a long-term time series resource, offering fine spatial detail at 500 m × 500 m. More information is available at the homepage of the National Cryosphere Desert Data Center of China (http://www.ncdc.ac.cn).

280 2.4.3 Meteorological and air quality data

To evaluate the model's performance concerning surface temperature and rainfall, which are important for snow simulation, we obtained meteorological data on temperature and precipitation from the National Climatic Data Center (NCDC) (https://www.ncdc.noaa.gov/). The NCDC has more than 400 ground stations in China, and data have been collected since 1942.

285

3 Results and Discussion

3.1 Meteorological simulations

The accuracy of snow simulation is largely influenced by temperature and precipitation. As a result, it is important to assess how well WRF-Chem performs in simulating these variables. WRF-

290 Chem does not directly simulate snowfall but instead uses a practical method in which precipitation occurring at temperatures less than 0 ℃ is considered snowfall.

Figure 2 depicts the 2 m temperature patterns across China simulated by WRF-Chem and observed, with average values from December 2017 to March 2018. Daily 2 m temperature data from December 2017 to March 2018 at 415 sites in China were sourced from the National Oceanic and

295 Atmospheric Administration (NOAA). Based on the graph, it is evident that the model accurately depicts the spatial patterns and fluctuations in the 2 m temperature, aligning well with the observed data. Furthermore, the simulation accurately represents the notable decrease in the 2 m temperature as latitude increases, ranging from near freezing levels to approximately -30°C.

Figure 3 displays the spatial distribution of precipitation observed and simulated by WRF-Chem

300 over China, averaged from December 2017 to March 2018. Daily precipitation observations from December 2017 to March 2018 at 415 sites in China were also obtained from NOAA. The results

indicate good agreement between the simulated and observed rainfall in the northern regions. However, there is a notable underestimation in the simulation for the southern regions of China. Nevertheless, since our primary focus is on the northern regions where snowfall mainly occurs, this underestimation

305 does not significantly impact our snow simulation. In the northeastern, northwestern, and Qinghai–Tibet Plateau regions of China, the temperatures are generally less than 0°C. Therefore, the precipitation in these areas can be considered snowfall. Notably, there is a slight underestimation of precipitation in Jilin and Liaoning Provinces in northeastern China, which could lead to a slight underestimation in the subsequent snow simulation.
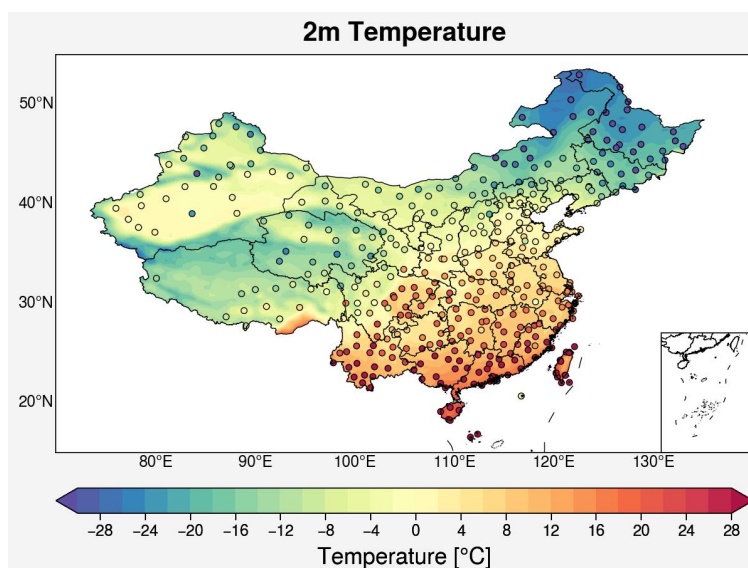
310

Figure 2. Spatial distribution of 2 m temperature observed and simulated by WRF-Chem over China averaged from December 2017 to March 2018. [Note: The observed values are represented by circles in the figure.]
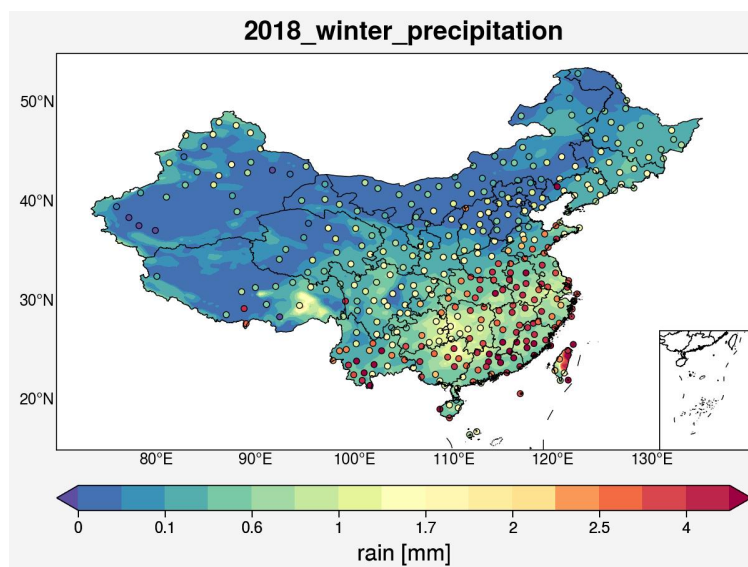
Figure 3. Spatial distribution of precipitation observed and simulated by WRF-Chem over China averaged from December 2017 to March 2018. [Note: The observed values are represented by circles in the figure.]

3.2 Snowpack simulations

3.2.1 Spatial distributions of snow cover

Before analyzing the patterns of light-absorbing impurities in snow, it is crucial to assess the simulated snow cover produced by WRF-Chem. Figure 4 shows the spatial patterns of snow cover (the percentage of land area with snow at each grid cell) from the WRF-Chem simulation (left column) and MODIS-based observational data (right column) from December 2017 to March 2018, providing the average results for each month. Here, snow cover is defined as the snow fraction [0-1], which represents the percentage of land area with snow at each grid point. Both simulations and observations indicate that snow cover is concentrated primarily in China's northeastern, northwestern, and Qinghai–Tibet Plateau regions. The distribution of snow cover generally follows the temperature pattern. Areas with lower temperatures tend to have greater snow cover. The highest snow cover percentage, up to 90%, is observed in the northeastern region. Both the observations and simulations reveal snow accumulations in central China in January 2018.
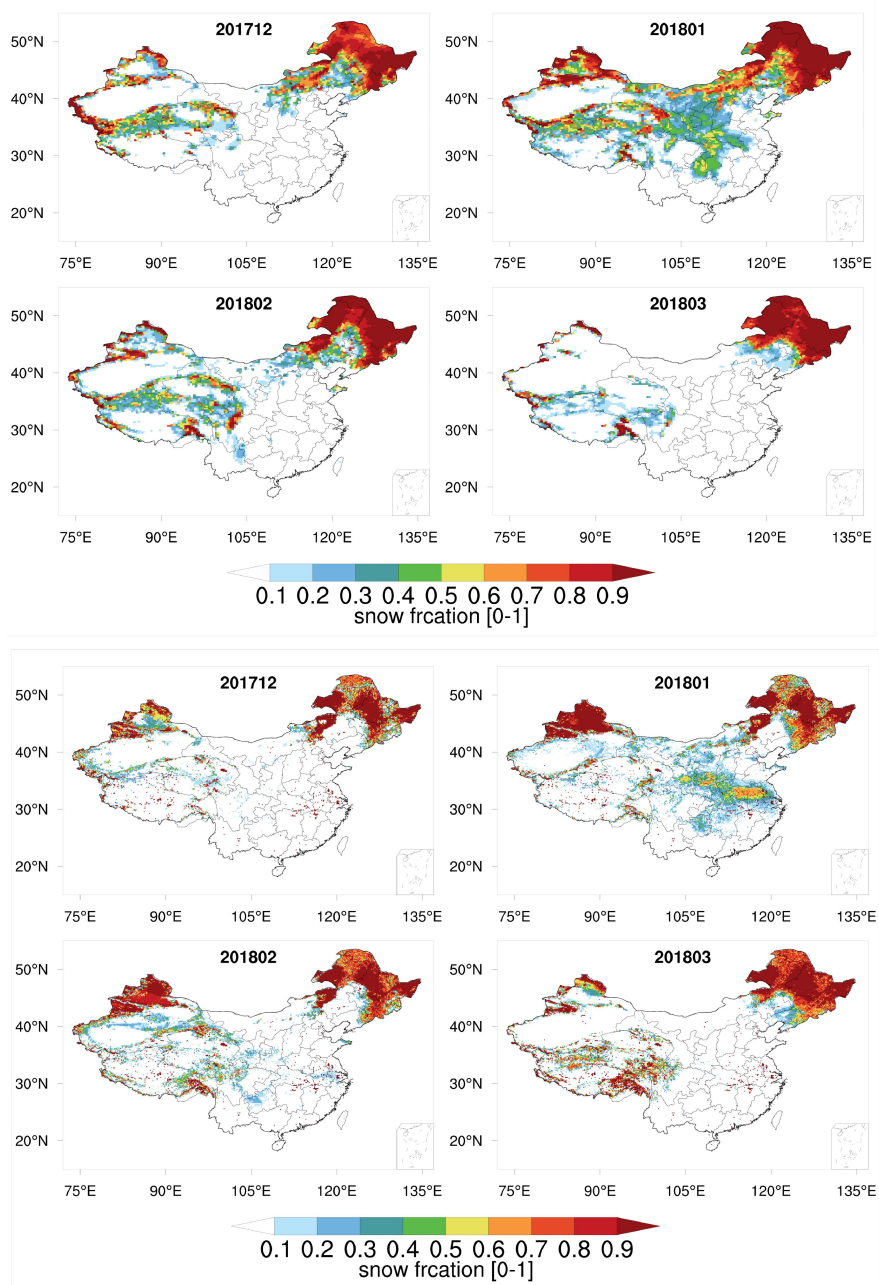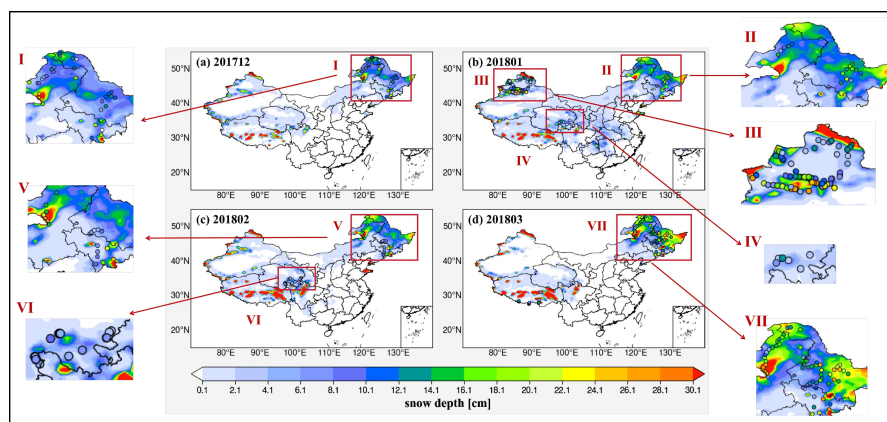
Figure 4. Spatial distribution of snow cover simulated by WRF-Chem (top) and observed from MODIS-based data (bottom) across China from December 2017 to March 2018. The data presented are monthly averages.

335

3.2.2 Snow depth

Figure 5 illustrates the simulated snow depth from December 2017 to March 2018 along with the
340 observations from the field campaign integrated into each panel. The background color in the figures
represents the monthly average of the simulation results, while the plotted dots indicate the observed
data for that month. In general, the simulation and observation results exhibit consistency in terms of
spatial distributions and magnitudes, both of which indicate that snow depth is deeper in a northly
direction. In particular, among the four months, January 2018 had the highest number of observations,
345 distributed across the northeastern, northwestern, and Tibet plateau regions of China. The observed data
for the other three months are primarily concentrated in the northeastern region of China. Detailed
comparison maps for specific regions can also be found in Fig. 5. Over time, the snow cover in the
northeastern region exhibits dynamic variations (I, III, V, and VII in Fig. 5). From December 2017 to
March 2018, there was a gradual increase in snow depth each month, reaching its maximum in March
350 2018. In January 2018, in the northeastern region, the model well captured the spatial variations in the
observed snow depths, with excellent agreement in both high- and low-value areas. (VII in Fig. 5). In
March 2018, extensive observational data were collected, primarily focused on the western Greater
Khingan Mountains and the Northeast China Plain in Northeast China. From the panel, we can observe
that the overall simulation performance is quite satisfactory, as it effectively captures the spatial
355 variations in snow depth. The simulation successfully reproduced high snowfall values around the
Hulunbuir area, located in the Inner Mongolia Autonomous Region, reaching up to 29 cm. The March
snow variations are clearly visible in the figure, with snow depths reaching more than 20 cm in both the
western Greater Khingan Mountains and the Northeast China Plain.

360 **Figure 5.** Spatial distribution of snow depth (cm) observed and simulated by WRF-Chem and across China from December 2017 to March 2018. [Note: The background color in each figure represents the monthly average of the simulation results, while all the observations for each month are embedded in each panel.]

365 **3.3 Modeling of DUST and BC concentrations in snow**

3.3.1 Spatiotemporal variability of Dust in snow

Figure 6 illustrates the pattern of dust concentration (mg/g) in the top snow layer simulated by WRF-Chem, presented in the top column. Additionally, in the absence of direct dust measurement data, we have graphed the concentration of the dust tracer calcium ions in the top layer of snow a simulated

370 by the WRF-Chem model together with the field campaign observations for each month, shown in the bottom column. From the figure, it is clear that there are significant differences between the dust distributions in each month. For example, in December 2017, the dust is mainly concentrated in the northwestern part of China, while in January 2018, it spreads to other parts of the northwest and northeast. In February 2018, the dust seems to be more evenly distributed across northern China, and in

375 March 2018, it is mainly found in the northeastern part of China. These variations are associated with the distribution of snow cover in each month. Overall, dust is primarily distributed across Northwest China, Mongolia, and Liaoning Province, corresponding with the distribution of dust sources (see Fig. S2). In regions near dust source, DSTS is highest (> 3 mg g^{-1}). As far away from the source region, DSTS gradually decreases. In Northeast and Central China, the concentration decreases to

380 approximately 10 µg g^{-1}, and at the further northern boundaries, the concentrations can even drop as low as ~100 ng g^{-1}.

The modeled calcium ion content in the snow was calculated based on the proportion of calcium carbonate in the GOCART dust emission mechanism used in WRF-Chem (Ginoux et al., 2001; Kok et al., 2014a; Kok et al., 2014b). Field-observed calcium ion concentrations in the top layer of snow (CAS)

385 are indicated by dots superimposed at the bottom of Fig 6. The simulated CAS values closely match the observations, effectively capturing the spatial variation and magnitude of the CAS. The simulation shows the highest CAS, exceeding 10 µg g^{-1}, across Northwest China (90–100°E, 40–50° N) in January 2018, where the DSTS is also the highest ((b) in Fig. 6. Moreover, the high CAS values simulated during this month align well with the actual measurements recorded, accurately capturing the overall

390 spatial variations. CAS and DSTS exhibit similar distribution patterns and are primarily concentrated in

the northern and northwestern regions of China, such as Inner Mongolia and Liaoning Province. These

areas are characterized by arid and semiarid climatic conditions and desert landscapes, increasing

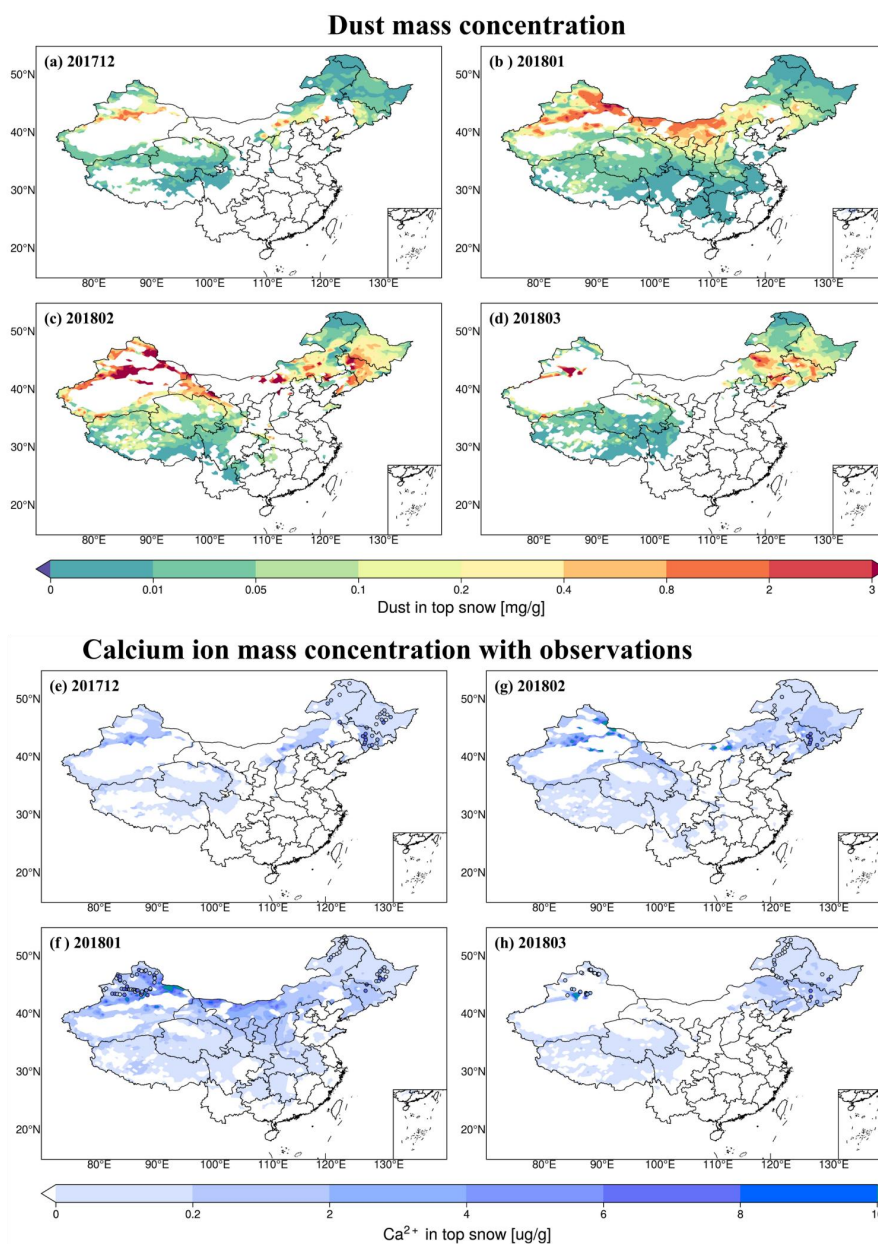susceptibility to the dispersal of dust particles.

Figure 6. Spatial distribution of dust concentration (mg/g) simulated by WRF-Chem in the top snow
layer (a, b, c and d) and calcium ion concentration simulated by WRF-Chem in the top snow layer with

395

the field campaign observations at specific locations embedded in each month (e, f, g and h) across China from December 2017 to March 2018.

400

3.3.2 Spatiotemporal variability of BC in snow

Figure 7 displays the modeled black carbon (BC) concentration distributions across space in the top layer of snow across China from December 2017 to March 2018, simulated by WRF-Chem. We do not have BC observations during the simulation period, however, using the same model, Zhao et al.

405 (2014) previously conducted BC simulations in Northeast China and compared the results with observational data, and the model agreed well with the observations. In the vicinity of approximately 40° N and 125° E in Northeast China, as depicted in Fig.7, the highest concentrations of BC in the top snow layer (BCS) reach more than 6000 ng g^{-1}. This region is characterized by significant snow cover and depth, as illustrated in Figs. 4 and 5. As far away from northeast China, the BCS decreases and

410 drops to less than 50 ng g^{-1} towards the northwest border of China. This finding aligns with the results of Zhao et al. (2014), who reported high BCSs in areas of dense industrial activity and reduced levels (30–50 ng g^{-1}) at more northerly latitudes in the northern reaches of China, around 51° N. The large spatial and temporal variations in BCS are influenced in part by the changes in snow conditions (Fig. 5) and its BC content as represented in the model. During the initial accumulation of snow, the mass of

415 BC within the snow is significantly less than the mass of the snow itself, leading to the lowest recorded BCS. Subsequently, the BCS progressively increases as snow accumulates and is influenced by deposition processes. As the snow begins to melt, BCS continues to rise due to dry deposition until the snow completely melts. Note that in Jan. 2018, a high concentration of BC was simulated in central China, which was due to the low snow accumulation at that time (i.e., low snowfall but high BC

420 emissions led to high snow BC content).
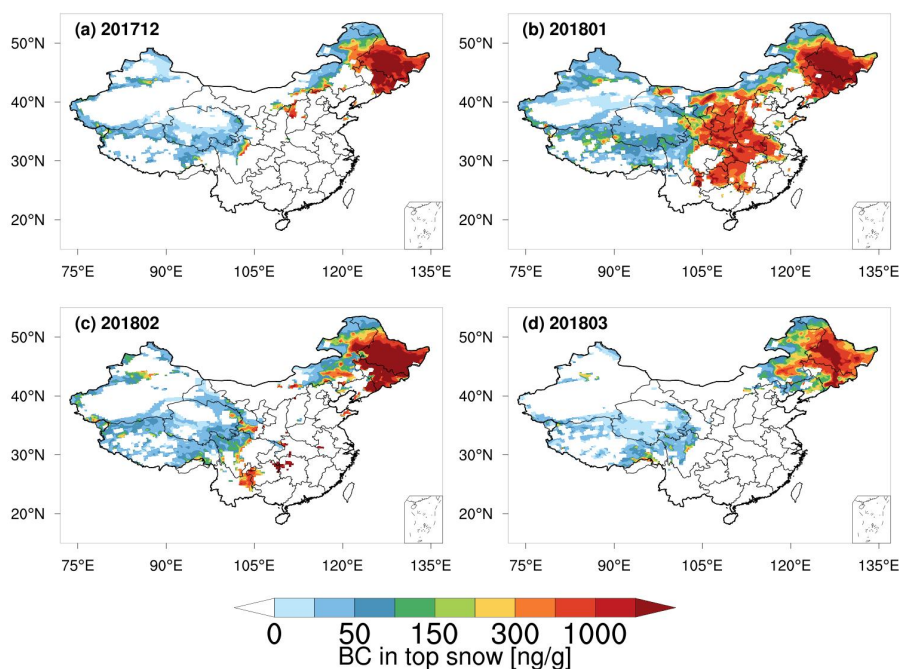
Geoscientific
Model Development
Discussions

Figure 7. Spatial distribution of BC concentration (ng/g) in the top snow layer simulated by WRF-Chem across China from December 2017 to March 2018. [Note: The background color in each figure represents the monthly average of the simulation.]

3.4 Snow nitrate simulations

3.4.1 Deposition fluxes of nitrate on snow

Snow nitrate concentration was calculated by incorporating dry and wet total nitrate (atmospheric gaseous and particulate nitrate) deposition fluxes into the SNICAR module in WRF-Chem. Therefore, before assessing the concentration of nitrate in the snowpack, it is necessary to evaluate the reasonableness of the model-derived deposition fluxes. The simulated spatial distributions of nitrate deposition via dry and wet processes on snow from December 2017 to March 2018 are shown in Fig. 8. Deposition fluxes only accumulate across snow-covered surfaces, both in space and time. To assess nitrate deposition fluxes in winter China, we initially compared our simulation results with findings from other simulation studies (Liu et al., 2022; Ma et al., 2023a; Zhao et al., 2015). Overall, our simulation results exhibit consistency in terms of the spatial distributions and magnitudes of atmospheric nitrate deposition. During the studied period spanning from December 2017 to March 2018, the monthly deposition flux of nitrate (including both dry and wet depositions of gaseous and

440 particulate nitrate) in China was approximately 0.17 ± 0.007 (mean $\pm 1\sigma$) kg N ha^{-1} month^{-1}. Among

them, dry deposition contributed approximately 0.07 ± 0.005 kg N ha^{-1} month^{-1}, while wet deposition

accounted for 0.09 ± 0.007 kg N ha^{-1} month^{-1}. Wet deposition comprised a slightly greater proportion,

constituting 56% of the total deposition flux. In comparison, Yu et al. (2019) utilized linear regression

and Kriging interpolation methods drawing upon data from the Nationwide Nitrogen Deposition

445 Monitoring Network (NNDMN), finding that the monthly dry deposition flux of nitrate (including both

gaseous and particulate nitrate) over China from 2011 to 2015 was approximately 0.27 ± 0.08 (mean $\pm$

1σ) kg N ha^{-1} month^{-1} and wet deposition flux was approximately 0.31 ± 0.23 kg N ha^{-1} month^{-1}. Note

this monthly average are values considering data from all 12 months but not only in winter. If

considering winter only means, the dry and wet deposition fluxes are (0.09 ± 0.03 kg N ha^{-1} month^{-1})

450 and (0.10 ± 0.07 kg N ha^{-1} month^{-1}), respectively, assuming the monthly means are approximately 1/3

of summer means according to previous nitrate deposition of seasonal research findings (Ma et al.,

2023b; Pan et al., 2012). In addition, we found two observation sites in Jilin and Liaoning provinces in

Northeast China from the NNDMN. At the Jilin site (124.83°E, 43.53°N), in winter months, the

simulated monthly dry deposition of nitrate (atmospheric gaseous and particulate nitrate, the same as

455 follows) was 0.07 ± 0.10 kg N ha^{-1} month^{-1}, and wet deposition was 0.16 ± 0.28 kg N ha^{-1} month^{-1},

with in the ranges of the observed values of 0.13 ± 0.03 kg N ha^{-1} month^{-1} for dry deposition and 0.28

± 0.11 kg N ha^{-1} month^{-1} for wet deposition. At the Liaoning site (121.58°E, 38.92°N), the simulated

dry deposition was 0.18 ± 0.17 kg N ha^{-1} month^{-1}, and wet deposition was 0.79 ± 0.32 kg N ha^{-1}

month^{-1}, while the observed dry deposition was 0.38 ± 0.18 kg N ha^{-1} month^{-1}, while wet deposition

460 was 0.35 ± 0.18 kg N ha^{-1} month^{-1}. Although at the Liaoning site, the modeled wet and dry deposition

fluxes are somewhat different from the observations, their sums (i.e., the total deposition fluxes) are

close to each other (0.97 ± 0.36 kg N ha^{-1} month^{-1} vs. 0.73 ± 0.25 kg N ha^{-1} month^{-1}) within the range

of uncertainties.
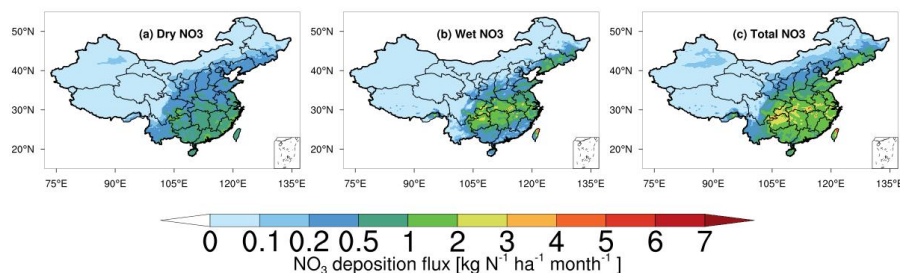
465   Figure 8. Spatial distribution of (a) dry, (b) wet, and (c) total (dry + wet) deposition fluxes (kg N ha^{-1} month^{-1}) of oxidized nitrogen (atmospheric gaseous plus particulate nitrate) on snow simulated by WRF-Chem in mainland China averaged over December 2017 to March 2018.

3.4.2 Nitrate concentrations and spatial distribution in snow

470   Figure 9 displays the nitrate concentration distributions across space in the top snow layer simulated by WRF-Chem averaged for December 2017 to March 2018, with the field campaign observations of nitrate concentration in the top snow layer (NITS). Among the four months, January 2018 had the highest number of observations, distributed across northeastern and northwestern China. The observed data for the other three months are primarily concentrated in the northeastern region of

475   China. During these four months, consistent patterns of change were identified, as the model simulating the highest NITS (> 15 µg g^{-1}) in the region spanning Northeast China (125–132° E, 40–47° N), mainly encompassing the provinces of Heilongjiang, Jilin, and Liaoning. In addition, as far away from northeast China, the NITS decreases and drop to less than 0.06 µg g^{-1} at the boundary of northern China. This finding aligns with our field campaign data, revealing elevated NITS levels (1.03–33.43 µg g^{-1}) in

480   areas characterized by heavy industrialization and lower concentrations (0.08–0.4 µg g^{-1}) in the northern regions of China (52° N). From a temporal perspective, there was a significant increase in the simulated NITS in northeastern Jilin Province from December 2017 to March 2018. This difference may be attributed to the monthly increase in simulated nitrate deposition in this region, while snowfall slightly decreased in the northeastern area during the same period.

485   The road trip during the campaign began in Inner Mongolia, which, compared to Northeast China, exhibits relatively lower pollution levels, with most observed NITS values below 1 µg g^{-1}. The cleanest snow samples, with concentrations in the tens of nanograms per gram range, were collected close to China's northern border, while polluted snow was obtained from the industrialized zones of Northeast China. The WRF-Chem simulation effectively reproduces the observed notable escalation in NITS

490   toward more polluted sites, from 0.08–0.4 µg g^{-1} at 51° N to more than 10 µg g^{-1} at 43° N. Both temporally and spatially, the simulation results generally align with the observations, albeit with some negative biases in relatively clean areas (e.g., Inner Mongolia).

The WRF-Chem model-simulated maximum values ranged from 7.11 to 16.58 µg g^{-1}, while the range of the simulated minimum values was between 0.06 and 0.21 µg g^{-1}. The observed maximum

495   values varied between 9.35 and 33.43 µg g^{-1}, with observed minimum values falling within the range of

0.09 to 0.51 µg g^{-1}. In addition to the results described above, we also calculated the overall average values for the four months. The simulation results indicate an average concentration of 2.72 ± 1.34 µg g^{-1}, whereas the observed four-month average concentration is 3.74 ± 5.42 µg g^{-1}. This conclusion aligns well with the results presented with the findings of Xue et al. (2020), who also conducted

500   observations on snowfall in northeastern China from December 2017 to March 2018. Covering the same period and region as ours, their results revealed maximum, minimum, and average nitrate concentrations in snow of 12.25, 0.08, and 3.34 ± 1.00 mg/L, respectively. Although our simulation shows a certain degree of underestimation at some sites compared to the observational results, the simulated results generally capture both the spatial trends and magnitudes seen in the data. Regarding

505   this underestimation, as illustrated in Figure 9, we note that there is a low bias for the NITS in high-pollution areas between December 2017 and January 2018. This discrepancy might be attributed to the accumulation processes within the snowpack. However, it is important to acknowledge that the model also encompasses various uncertainties, such as incomplete representations of emission sources, nitrate production mechanisms, deposition processes, and aerosol scavenging in snow.

510   Given the substantial fluctuations in the temporal patterns of annual snowpack accumulation and the challenges in accurately predicting the occurrence of weather phenomena, aerosol releases, and deposition processes, it is judicious to compare data by utilizing the long-standing averages obtained from both actual and modeled NITS datasets across an extended timespan. Additionally, further comparisons were conducted by comparing the averaged model results within the same day with the

515   values observed at each site on the same day. However, these analyses showed no significant alterations (data not presented). The significant temporal fluctuations in NITS may also pose challenges when comparing monthly average values from model simulation result with field observations at particular times, a widely used method across global atmospheric modeling research (Huang et al., 2011; Qian et al., 2014; Zhao et al., 2014). The sample sites within industrial source regions are subject to increasing

520   relative biases, with the model typically underestimating the NITS at these locations. In addition to the uncertainty in the snow accumulation process mentioned above, this difference may also be related to the challenge the model faces in capturing fine-scale variability within grid cells, which tends to be more pronounced in regions with high emissions compared to relatively clean areas.
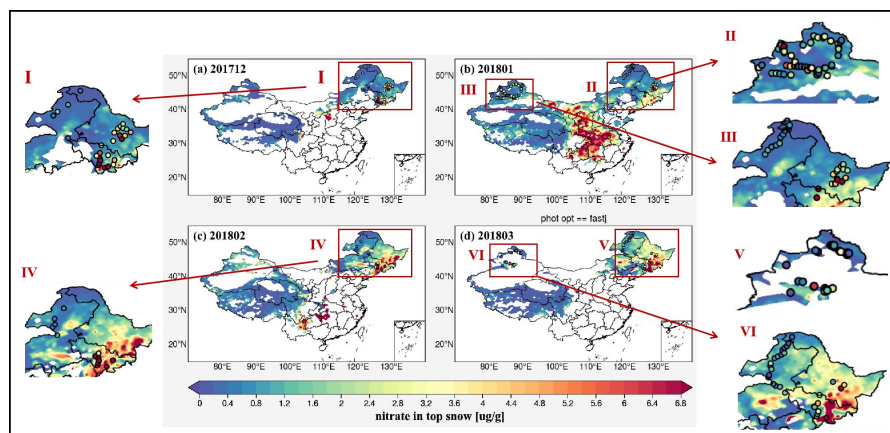
Figure 9. Spatial distribution of nitrate concentration in the top snow layer observed and simulated by WRF-Chem across China from December 2017 to March 2018. [Note: The background color in each figure represents the monthly average of the simulation results, while all the observations for each month are embedded in each panel.]

4 Conclusion

In this study, the WRF-Chem model was used to simulate snow cover, snow depth, and snow impurities including BC, dust and nitrate concentration in winter 2017-2018 across China. Field observations covering the same regions and periods were used to evaluate the ability of the model. Overall, the model effectively replicates the observed scale and spatial fluctuations of surface temperature, snow coverage, snow impurities, and aerosol levels within the snow. In particular, we thoroughly evaluated all simulation results with observations. Firstly, the model accurately represented the spatial trends and magnitudes of snow cover and snow depth. Secondly, our simulation results for the light-absorbing impurities BC and DUST were validated through various assessment methods. Thirdly, we conducted a critical assessment of the deposition flux assumption for the simulation of snow nitrate and confirmed the validity of the results before assessing the simulation outcomes. Overall, the spatial trends and concentration levels for snow nitrate were well represented, with slight underestimations observed in high-pollution areas.

The discrepancies in impurity concentrations between the model and observations could be due to the incomplete chemical mechanisms regarding atmospheric N transformations in the model and may also be partly caused by the relatively coarse model resolution, w which may not adequately capture the heterogeneous spatial distributions of snow and its impurity concentrations. Additionally, numerous other variables and processes contribute to the uncertainty surrounding simulations of snow and

aerosols contents within snowpack, including but not limited on the snow accumulation processes, the primary emission sources of impurity precursors, the gas and aerosol scavenging in the snow, and etc.

550 But overall, the model demonstrates its ability in capturing the temporal and spatial variations in snow impurity concentrations including nitrate in Northern China. The considerable daily and diurnal fluctuations in simulated NITS emphasize the need for caution when comparing average values derived from the model with observations, as practiced in certain global modeling analyses. (Huang et al., 2011; Qian et al., 2014; Zhao et al., 2014).

555 It's worth mentioning that despite the overall evaluation of simulated spatial patterns of snow depth and aerosol concentrations within the snowpack against observations, discrepancies persist in simulating snow impurities, even though they have been fully quantified. Such biases could stem from uncertainties across various snow model processes, the primary emission sources of impurity precursors from atmosphere model, the gas and aerosol scavenging in the snow, and etc. Ensuring 560 accurate representation of aerosol contents within snow requires the model to effectively simulate the life cycle of aerosols within snowpack, as highlighted in previous studies by Flanner et al. (2012) and Qian et al. (2014). Furthermore, uncertainties in the SNICAR model parameters must be quantified and constrained through observational data. Additionally, it is crucial for the model to precisely replicate the atmospheric aerosol life cycle, encompassing the faithful representation of atmospheric aerosol 565 levels and the accurate treatment of deposition mechanisms. Improvements in such model parameters and mechanisms would be necessary to further improve the agreement with observations.

Given the reasonable agreements between the model and observations, we will further incorporate snow nitrate photolysis and the subsequent emissions of NO_2 and/or HONO to the overlying atmosphere, investigating the potential disturbs on local to regional atmospheric chemistry with focuses 570 on aerosol burden which is important for atmospheric and snow radiative balances in snow cover regions, and on the potential effects on air quality originating from the winter snow cover to the downwind regions in Northern China.

Code and data availability

The release version of WRF-Chem can be downloaded from 575 http://www2.mmm.ucar.edu/wrf/users/download/get_source.html. The modified version of WRF-Chem used in this study is archived on Zenodo at https://doi.org/10.5281/zenodo.10586762. All the original

Author contributions

580 LG conceived the study, XW conducted the model experiments and analysed the results under the supervision of LG and CZ; TC, SY and JW provided the field observational data; XW drafted the manuscript under the supervision of LG; all authors contributed to the discussion and the final version of the manuscript.

Competing interests

585 The authors declare that they have no conflict of interest.

Acknowledgements

References

An, Y., Xu, J., Liu, Y., Li, X., Zhao, H., and Kang, S.: Concentrations, Compositions, and Deposition
595 Rates of Dissolved Nitrogen in Western China: Insights From Snow Records, Frontiers in Environmental Science, 9, https://doi.org/10.3389/fenvs.2021.827456, 2022.

Barbero, A., Savarino, J., Grilli, R., Blouzon, C., Picard, G., Frey, M. M., Huang, Y., and Caillon, N.: New Estimation of the NOx Snow-Source on the Antarctic Plateau, Journal of Geophysical Research: Atmospheres, 126, e2021JD035062, https://doi.org/10.1029/2021JD035062, 2021.

600 Binkowski, F. S. and Shankar, U.: The Regional Particulate Matter Model: 1. Model description and preliminary results, Journal of Geophysical Research: Atmospheres, 100, 26191-26209, https://doi.org/10.1029/95JD02093, 1995.

Bouwman, A. F.: Nitrogen oxides and tropical agriculture, Nature, 392, 866-867, https://doi.org/10.1038/31809, 1998.

605 Brandt, R. E., Warren, S. G., and Clarke, A. D.: A controlled snowmaking experiment testing the relation between black carbon content and reduction of snow albedo, Journal of Geophysical Research: Atmospheres, 116, https://doi.org/10.1029/2010JD015330, 2011.

Chapman, E., Gustafson, W. I., Easter, R. C., Barnard, J. C., Ghan, S. J., Pekour, M. S., and Fast, J. D.: Coupling aerosol-cloud-radiative processes in the WRF-Chem model: Investigating the radiative
610 impact of elevated point sources, Atmospheric Chemistry and Physics, 9, 945-964, https://doi.org/10.5194/acp-9-945-2009, 2008.

Che, T.: Chinese guidelines for snowpack observation in the field[M], Beijing: Science Press2020.

Che, T., Dai, L., Xiao, L., and Wang, J.: A dataset for in situ snow characteristics in China (2017–2020), China Scientific Data, 7, http://doi.org/10.11922/11-6035.ncdc.2022.0001.zh, 2022.

615 Chen, Q., Edebeli, J., McNamara, S. M., Kulju, K. D., May, N. W., Bertman, S. B., Thanekar, S., Fuentes, J. D., and Pratt, K. A.: HONO, Particulate Nitrite, and Snow Nitrite at a Midlatitude Urban Site during Wintertime, ACS Earth and Space Chemistry, 3, 811-822, https://doi.org/10.1021/acsearthspacechem.9b00023, 2019.

Chu, L. and Anastasio, C.: Quantum Yields of Hydroxyl Radical and Nitrogen Dioxide from the
620 Photolysis of Nitrate on Ice, Journal of Physical Chemistry A, 107, 9594-9602, https://doi.org/10.1021/jp0349132, 2003.

Doherty, S. J., Grenfell, T. C., Forsström, S., Hegg, D. L., Brandt, R. E., and Warren, S. G.: Observed vertical redistribution of black carbon and other insoluble light-absorbing particles in melting snow, Journal of Geophysical Research: Atmospheres, 118, 5553-5569,
625 https://doi.org/10.1002/jgrd.50235, 2013.

Dominé, F. and Shepson, P. B.: Air-Snow Interactions and Atmospheric Chemistry, Science, 297, 1506-1510, https://doi.org/10.1126/science.1074610, 2002.

Du, Q., Zhao, C., Zhang, M., Dong, X., Chen, Y., Liu, Z., Hu, Z., Zhang, Q., Li, Y., Yuan, R., and Miao, S.: Modeling diurnal variation of surface PM2.5 concentrations over East China with WRF-Chem:
630 impacts from boundary-layer mixing and anthropogenic emission, Atmos. Chem. Phys., 20, 2839-2863, https://doi.org/10.5194/acp-20-2839-2020, 2020.

Easter, R. C., Ghan, S. J., Zhang, Y., Saylor, R. D., Chapman, E. G., Laulainen, N. S., Abdul-Razzak, H., Leung, L. R., Bian, X., and Zaveri, R. A.: MIRAGE: Model description and evaluation of aerosols and trace gases, Journal of Geophysical Research: Atmospheres, 109,
635 https://doi.org/10.1029/2004JD004571, 2004.

EICHLER, A., SCHWIKOWSKI, M., and GÄGGELER, H. W.: Meltwater-induced relocation of chemical species in Alpine firn, Tellus B, 53, 192-203, https://doi.org/10.1034/j.1600-0889.2001.d01-15.x, 2001.

Flanner, M. G. and Zender, C. S.: Snowpack radiative heating: Influence on Tibetan Plateau
640 climate, Geophysical Research Letters, 32, https://doi.org/10.1029/2004GL022076, 2005.

Flanner, M. G., Zender, C. S., Randerson, J. T., and Rasch, P. J.: Present-day climate forcing and response from black carbon in snow, Journal of Geophysical Research, 112, https://doi.org/10.1029/2006JD008003, 2007.

Flanner, M. G., Liu, X., Zhou, C., Penner, J. E., and Jiao, C.: Enhanced solar energy absorption by
645 internally-mixed black carbon in snow grains, Atmos. Chem. Phys., 12, 4699-4721, https://doi.org/10.5194/acp-12-4699-2012, 2012.

Flanner, M. G., Shell, K. M., Barlage, M., Perovich, D. K., and Tschudi, M. A.: Radiative forcing and albedo feedback from the Northern Hemisphere cryosphere between 1979 and 2008, Nature Geoscience, 4, 151-155, https://doi.org/10.1038/ngeo1062, 2011.

650 Flanner, M. G., Zender, C. S., Hess, P. G., Mahowald, N. M., Painter, T. H., Ramanathan, V., and Rasch, P. J.: Springtime warming and reduced snow cover from carbonaceous particles, Atmos. Chem. Phys., 9, 2481-2497, https://doi.org/10.5194/acp-9-2481-2009, 2009.

Ginoux, P., Chin, M., Tegen, I., Prospero, J. M., Holben, B., Dubovik, O., and Lin, S.-J.: Sources and distributions of dust aerosols simulated with the GOCART model, Journal of Geophysical
655 Research: Atmospheres, 106, 20255-20273, https://doi.org/10.1029/2000JD000053, 2001.

Grannas, A. M., Jones, A. E., Dibb, J., Ammann, M., Anastasio, C., Beine, H. J., Bergin, M., Bottenheim, J., Boxe, C. S., Carver, G., Chen, G., Crawford, J. H., Dominé, F., Frey, M. M., Guzmán, M. I., Heard, D. E., Helmig, D., Hoffmann, M. R., Honrath, R. E., Huey, L. G., Hutterli, M., Jacobi, H. W., Klán, P., Lefer, B., McConnell, J., Plane, J., Sander, R., Savarino, J., Shepson, P. B., Simpson, W.
660 R., Sodeau, J. R., von Glasow, R., Weller, R., Wolff, E. W., and Zhu, T.: An overview of snow photochemistry: evidence, mechanisms and impacts, Atmos. Chem. Phys., 7, 4329-4373, https://doi.org/10.5194/acp-7-4329-2007, 2007.

Hadley, O. L. and Kirchstetter, T. W.: Black-carbon reduction of snow albedo, Nature Climate Change, 2, 437-440, https://doi.org/10.1038/nclimate1433, 2012.

665 Hall, S. J. and Matson, P. A.: Nitrogen oxide emissions after nitrogen additions in tropical forests, Nature, 400, 152-155, https://doi.org/10.1038/22094, 1999.

Hao, X., Huang, G., Zheng, Z., Sun, X., Ji, W., Zhao, H., Wang, J., Li, H., and Wang, X.: Development and validation of a new MODIS snow-cover-extent product over China, Hydrology and Earth System Sciences, 26, 1937-1952, https://doi.org/10.5194/hess-26-1937-2022, 2022.

670 He, C., Liou, K.-N., Takano, Y., Yang, P., Qi, L., and Chen, F.: Impact of Grain Shape and Multiple Black Carbon Internal Mixing on Snow Albedo: Parameterization and Radiative Effect Analysis, Journal of Geophysical Research: Atmospheres, 123, 1253-1268, https://doi.org/10.1002/2017JD027752, 2018.

Huang, J., Fu, Q., Zhang, W., Wang, X., Zhang, R., Ye, H., and Warren, S. G.: Dust and Black
675 Carbon in Seasonal Snow Across Northern China, Bulletin of the American Meteorological Society, 92, 175-181, https://doi.org/10.1175/2010BAMS3064.1, 2011.

Jiang, Z., Alexander, B., Savarino, J., Erbland, J., and Geng, L.: Impacts of the photo-driven post-depositional processing on snow nitrate and its isotopes at Summit, Greenland: a model-based study, The Cryosphere, 15, 4207-4220, https://doi.org/10.5194/tc-15-4207-2021, 2021.

680 Jin, J. and Wen, L.: Evaluation of snowmelt simulation in the Weather Research and Forecasting model, Journal of Geophysical Research: Atmospheres, 117, https://doi.org/10.1029/2011JD016980, 2012.

Kok, J. F.: A scaling theory for the size distribution of emitted dust aerosols suggests climate models underestimate the size of the global dust cycle, Proceedings of the National Academy of
685 Sciences, 108, 1016-1021, https://doi.org/10.1073/pnas.1014798108, 2011.

Kok, J. F., Albani, S., Mahowald, N. M., and Ward, D. S.: An improved dust emission model – Part 2: Evaluation in the Community Earth System Model, with implications for the use of dust source functions, Atmos. Chem. Phys., 14, 13043-13061, https://doi.org/10.5194/acp-14-13043-2014, 2014a.

690 Kok, J. F., Mahowald, N. M., Fratini, G., Gillies, J. A., Ishizuka, M., Leys, J. F., Mikami, M., Park, M. S., Park, S. U., Van Pelt, R. S., and Zobeck, T. M.: An improved dust emission model – Part 1: Model description and comparison against measurements, Atmospheric Chemistry and Physics, 14, 13023-13041, https://doi.org/10.5194/acp-14-13023-2014, 2014b.

Lawrence, D. M., Oleson, K. W., Flanner, M. G., Thornton, P. E., Swenson, S. C., Lawrence, P. J.,
695 Zeng, X., Yang, Z.-L., Levis, S., Sakaguchi, K., Bonan, G. B., and Slater, A. G.: Parameterization improvements and functional and structural advances in Version 4 of the Community Land Model, Journal of Advances in Modeling Earth Systems, 3, https://doi.org/10.1029/2011MS00045, 2011.

Legrand, M. and Mayewski, P. A.: Glaciochemistry of polar ice cores: A review, Reviews of
700   Geophysics, 35, 219 - 243, https://doi.org/10.1029/96RG03527, 1997.

Li, D., Oganov, A. R., Dong, X., Zhou, X.-F., Zhu, Q., Qian, G., and Dong, H.: Nitrogen oxides
under pressure: stability, ionization, polymerization and superconductivity, Scientific Reports, 5,
16311, https://doi.org/10.1038/srep16311, 2015.

Li, M., Zhang, Q., Kurokawa, J. I., Woo, J. H., He, K., Lu, Z., Ohara, T., Song, Y., Streets, D. G.,
705   Carmichael, G. R., Cheng, Y., Hong, C., Huo, H., Jiang, X., Kang, S., Liu, F., Su, H., and Zheng, B.:
MIX: a mosaic Asian anthropogenic emission inventory under the international collaboration
framework of the MICS-Asia and HTAP, Atmos. Chem. Phys., 17, 935-963,
https://doi.org/10.5194/acp-17-935-2017, 2017a.

Li, R., Dong, X., Guo, J., Fu, Y., Zhao, C., Wang, Y., and Min, Q.: The implications of dust ice nuclei
710   effect on cloud top temperature in a complex mesoscale convective system, Scientific Reports, 7,
13826, https://doi.org/10.1038/s41598-017-12681-0, 2017b.

Liu, M., Shang, F., Lu, X., Huang, X., Song, Y., Liu, B., Zhang, Q., Liu, X., Cao, J., Xu, T., Wang, T., Xu,
Z., Xu, W., Liao, W., Kang, L., Cai, X., Zhang, H., Dai, Y., and Zhu, T.: Unexpected response of
nitrogen deposition to nitrogen oxide controls and implications for land carbon sink, Nat
715   Commun, 13, 3126, https://doi.org/10.1038/s41467-022-30854-y, 2022.

Logan, J. A.: Nitrogen oxides in the troposphere: Global and regional budgets, Journal of
Geophysical Research: Oceans, 88, 10785-10807, https://doi.org/10.1029/JC088iC15p10785,
1983.

Ma, M., Zheng, B., Xu, W., Cao, J., Zhou, K., and Zhao, Y.: Trend and Interannual Variations of
720   Reactive Nitrogen Deposition in China During 2008–2017 and the Roles of Anthropogenic
Emissions and Meteorological Conditions, Journal of Geophysical Research: Atmospheres, 128,
https://doi.org/10.1029/2022JD037489, 2023a.

Ma, M., Zheng, B., Xu, W., Cao, J., Zhou, K., and Zhao, Y.: Trend and Interannual Variations of
Reactive Nitrogen Deposition in China During 2008–2017 and the Roles of Anthropogenic
725   Emissions and Meteorological Conditions, Journal of Geophysical Research: Atmospheres, 128,
e2022JD037489, https://doi.org/10.1029/2022JD037489, 2023b.

Moore, J. C., Grinsted, A., Kekonen, T., and Pohjola, V.: Separation of melting and environmental
signals in an ice core with seasonal melt, Geophysical Research Letters, 32,
https://doi.org/10.1029/2005GL023039, 2005.

730   Nelson, B. S., Bryant, D. J., Alam, M. S., Sommariva, R., Bloss, W. J., Newland, M. J., Drysdale, W. S.,
Vaughan, A. R., Acton, W. J. F., Hewitt, C. N., Crilley, L. R., Swift, S. J., Edwards, P. M., Lewis, A. C.,
Langford, B., Nemitz, E., Shivani, Gadi, R., Gurjar, B. R., Heard, D. E., Whalley, L. K., Şahin, Ü. A.,
Beddows, D. C. S., Hopkins, J. R., Lee, J. D., Rickard, A. R., and Hamilton, J. F.: Extreme
Concentrations of Nitric Oxide Control Daytime Oxidation and Quench Nocturnal Oxidation
735   Chemistry in Delhi during Highly Polluted Episodes, Environmental Science & Technology Letters,
10, 520-527, https://doi.org/10.1021/acs.estlett.3c00171, 2023.

Oleson, K., Lawrence, D., B, G., Flanner, M., Kluzek, E., Lawrence, P., Levis, S., Swenson, S.,
Thornton, E., Feddema, J., Heald, C., Lamarque, J.-F., Niu, G.-Y., Qian, T., Running, S., Sakaguchi,
K., Yang, Z.-L., Zeng, X., and Zeng, X.: Technical Description of version 4.0 of the Community
740   Land Model (CLM), http://doi.org/10.5065/D6FB50WZ, 2010a.

Oleson, K. W., Lawrence, D. M., Bonan, G. B., Flanner, M. G., Kluzek, E., Lawrence, P. J., Levis, S.,
Swenson, S. C., Thornton, P. E., Dai, A., Decker, M., Dickinson, R., Feddema, J., Heald,, C. L., H., F.,

Lamarque, J.-F., Mahowald, N., Niu, G.-Y.,, and Qian, T., Randerson, J., Running, S., Sakaguchi, K., Slater, A., Stöckli, R., Wang, A., Yang, Z.-L., Zeng, X., and Zeng, X: Technical Description of

745 version 4.0 of the Community Land Model (CLM), National Center for Atmospheric Research, http://doi.org/10.5065/D6FB50WZ, 2010b.

Pan, Y. P., Wang, Y. S., Tang, G. Q., and Wu, D.: Wet and dry deposition of atmospheric nitrogen at ten sites in Northern China, Atmospheric Chemistry and Physics, 12, 6515-6535, https://doi.org/10.5194/acp-12-6515-2012, 2012.

750 Picard, G., Domine, F., Krinner, G., Arnaud, L., and Lefebvre, E.: Inhibition of the positive snow-albedo feedback by precipitation in interior Antarctica, Nature Climate Change, 2, 795-798, 10.1038/nclimate1590, 2012.

Qian, Y., Wang, H., Zhang, R., Flanner, M. G., and Rasch, P. J.: A sensitivity study on modeling black carbon in snow and its radiative forcing over the Arctic and Northern China, Environmental

755 Research Letters, 9, 064001, https://doi.org/10.1088/1748-9326/9/6/064001, 2014.

Toon, O. B., McKay, C. P., Ackerman, T. P., and Santhanam, K.: Rapid calculation of radiative heating rates and photodissociation rates in inhomogeneous multiple scattering atmospheres, Journal of Geophysical Research: Atmospheres, 94, 16287-16301, https://doi.org/10.1029/JD094iD13p16287, 1989.

760 Wang, X. and Chen, R.: Influence of snow cover on soil freeze depth across China, Geoderma, 428, https://doi.org/10.1016/j.geoderma.2022.11619, 2022.

Wendl, I. A., Eichler, A., Isaksson, E., Martma, T., and Schwikowski, M.: 800-year ice-core record of nitrogen deposition in Svalbard linked to ocean productivity and biogenic emissions, Atmos. Chem. Phys., 15, 7287-7300, https://doi.org/10.5194/acp-15-7287-2015, 2015.

765 Wiedinmyer, C., Akagi, S. K., Yokelson, R. J., Emmons, L. K., Al-Saadi, J. A., Orlando, J. J., and Soja, A. J.: The Fire INventory from NCAR (FINN): a high resolution global model to estimate the emissions from open burning, Geosci. Model Dev., 4, 625-641, 10.5194/gmd-4-625-2011, 2011.

Wiscombe, W. J. and Warren, S. G.: A Model for the Spectral Albedo of Snow. I: Pure Snow, Journal of Atmospheric Sciences, 37, 2712-2733, https://doi.org/10.1175/1520-

770 0469(1980)037<2712:AMFTSA>2.0.CO;2, 1980.

Xue, H., Chen, W., Li, M., Liu, B., Li, G., and Han, X.: Assessment of major ions and trace elements in snow: A case study across northeastern China, 2017-2018, Chemosphere, 251, 126328, https://doi.org/10.1016/j.chemosphere.2020.126328, 2020.

Yu, G., Jia, Y., He, N., Zhu, J., Chen, Z., Wang, Q., Piao, S., Liu, X., He, H., Guo, X., Wen, Z., Li, P.,

775 Ding, G., and Goulding, K.: Stabilization of atmospheric nitrogen deposition in China over the past decade, Nature Geoscience, 12, 424-429, https://doi.org/10.1038/s41561-019-0352-4, 2019.

Yu, K., Keller, C. A., Jacob, D. J., Molod, A. M., Eastham, S. D., and Long, M. S.: Errors and improvements in the use of archived meteorological data for chemical transport modeling: an

780 analysis using GEOS-Chem v11-01 driven by GEOS-5 meteorology, Geosci Model Dev, 11, 305-319, https://doi.org/10.5194/gmd-11-305-2018, 2018.

Zatko, M., Geng, L., Alexander, B., Sofen, E., and Klein, K.: The impact of snow nitrate photolysis on boundary layer chemistry and the recycling and redistribution of reactive nitrogen across Antarctica and Greenland in a global chemical transport model, Atmos. Chem. Phys., 16, 2819-

785 2842, https://doi.org/10.5194/acp-16-2819-2016, 2016a.

Zatko, M., Erbland, J., Savarino, J., Geng, L., Easley, L., Schauer, A., Bates, T., Quinn, P. K., Light, B., Morison, D., Osthoff, H. D., Lyman, S., Neff, W., Yuan, B., and Alexander, B.: The magnitude of the snow-sourced reactive nitrogen flux to the boundary layer in the Uintah Basin, Utah, USA, Atmos. Chem. Phys., 16, 13837-13851, https://doi.org/10.5194/acp-16-13837-2016, 2016b.

790 Zatko, M. C., Grenfell, T. C., Alexander, B., Doherty, S. J., Thomas, J. L., and Yang, X.: The influence of snow grain size and impurities on the vertical profiles of actinic flux and associated NOx emissions on the Antarctic and Greenland ice sheets, Atmos. Chem. Phys., 13, 3547-3567, https://doi.org/10.5194/acp-13-3547-2013, 2013.

Zaveri, R. A. and Peters, L. K.: A new lumped structure photochemical mechanism for large-scale

795 applications, Journal of Geophysical Research: Atmospheres, 104, 30387-30415, https://doi.org/10.1029/1999JD900876, 1999.

Zaveri, R. A., Easter, R. C., Fast, J. D., and Peters, L. K.: Model for Simulating Aerosol Interactions and Chemistry (MOSAIC), Journal of Geophysical Research: Atmospheres, 113, https://doi.org/10.1029/2007JD008782, 2008.

800 Zhang, R., Hegg, D. A., Huang, J., and Fu, Q.: Source attribution of insoluble light-absorbing particles in seasonal snow across northern China, Atmos. Chem. Phys., 13, 6091-6099, https://doi.org/10.5194/acp-13-6091-2013, 2013.

Zhao, C., Ruby Leung, L., Easter, R., Hand, J., and Avise, J.: Characterization of speciated aerosol direct radiative forcing over California, Journal of Geophysical Research: Atmospheres, 118,

805 2372-2388, https://doi.org/10.1029/2012JD018364, 2013a.

Zhao, C., Chen, S., Leung, L. R., Qian, Y., Kok, J. F., Zaveri, R. A., and Huang, J.: Uncertainty in modeling dust mass balance and radiative forcing from size parameterization, Atmos. Chem. Phys., 13, 10733-10753, https://doi.org/10.5194/acp-13-10733-2013, 2013b.

Zhao, C., Liu, X., Leung, L. R., Johnson, B., McFarlane, S. A., Gustafson Jr, W. I., Fast, J. D., and

810 Easter, R.: The spatial distribution of mineral dust and its shortwave radiative forcing over North Africa: modeling sensitivities to dust emissions and aerosol size treatments, Atmos. Chem. Phys., 10, 8821-8838, https://doi.org/10.5194/acp-10-8821-2010, 2010.

Zhao, C., Hu, Z., Qian, Y., Ruby Leung, L., Huang, J., Huang, M., Jin, J., Flanner, M. G., Zhang, R., Wang, H., Yan, H., Lu, Z., and Streets, D. G.: Simulating black carbon and dust and their radiative

815 forcing in seasonal snow: a case study over North China with field campaign measurements, Atmos. Chem. Phys., 14, 11475-11491, https://doi.org/10.5194/acp-14-11475-2014, 2014.

Zhao, Y., Zhang, L., Pan, Y., Wang, Y., Paulot, F., and Henze, D. K.: Atmospheric nitrogen deposition to the northwestern Pacific: seasonal variation and source attribution, Atmos. Chem. Phys., 15, 10905-10924, https://doi.org/10.5194/acp-15-10905-2015, 2015.

820 Zou, Y., Sun, P., Ma, Z., Lv, Y., and Zhang, Q.: Snow Cover in the Three Stable Snow Cover Areas of China and Spatio-Temporal Patterns of the Future, Remote Sensing, 14, https://doi.org/10.3390/rs14133098, 2022.